Soft Matter

Accepted Manuscript

ROYAL SOCIETY OF CHEMISTRY

www.rsc.org/softmatter

Stability of double twisted structure in spherical cholesteric droplets

Jun Yoshioka*, Fumiya Ito and Yuka Tabe

Abstract

We found for the first time the stabilization of double twisted structure in cholesteric liquid crystals confined to small spherical droplets with weak anchoring condition. The direct observation of the droplets with polarized microscope revealed the physical properties of the structure. The experimental results showed the stability of the double twisted structure is determined by the relationship between the helical pitch length and the droplet size. We theoretically analyzed the structural stability by the calculation of the Frank elastic free energy including the surface elastic term, and succeed in explaining the experimental results. In this paper, we conclude the stability of the double twisted structure is determined by the competition between the surface and the bulk elasticity.

I. Introduction

When chirality is introduced to the nematic (N) liquid crystalline phase, it transits to the cholesteric (Ch) phase with a single helix structure (Fig.1(a)). However, the single helix is not always the most stable, and other director configurations can be formed according to physical or chemical conditions. One such example is the cholesteric blue phase which has recently received a lot of attention for realizing a three-dimensional laser (3D BP laser) and a next-generation high-speed display (BPLC display)[1–4]. The blue phase is formed by the cylindrical structures called ‘double twist cylinder (DTC)’, and the phase is categorized into BP I-III according to the array of the DTC: in the BP I and II, 3-dimensional lattice structure is

constructed by the DTC, on the other hand, the BP III is suggested to be amorphous[5-7]. In addition, it has been theoretically predicted novel 2-dimensional lattice structures are formed by the DTC when the BP I or II is confined to thin films[8]. On the other hand, the DTC is constructed by the lamination of the double twisted structure where the helical axes are radially extending within a plane[5,6,9] as shown in Fig.1(b). Thus, the physical properties of the blue phase should strongly depend on the stability of the double twisted structure itself, which, however, is not well studied experimentally. This is because the size of the DTC is too small for the experimental analysis: the diameter of the DTC is typically several hundreds of nanometer, which is not appropriate to be directly examined by convenient observation method such as polarized optical, confocal fluorescence, or reflection microscopy. To analyze the stability of the double twisted structure directly, we need to realize the structure in larger systems such as the micrometer-scale confined systems[10-17], colloidal systems[18,19], and so on.

As an example of the realization of the double twisted structure in micrometer-scaled systems, it has been reported the structure is stabilized when confined to cylindrical cavities under strong planer anchoring condition[10,11] this is reasonable because the double twisted structure is cylindrically symmetric. Also in the systems confined to spheres, several experiments and numerical calculation show the double twisted structure is realized under the strong planar anchoring condition[12,13]. In these systems, when the droplet radius R is smaller than the helical pitch length P, the double twisted structure is stable. However, when R goes beyond P, it transits into 'Frank-Pryce structure' or 'radial spherical structure' (RSS), where the helical axes are extending radially and 3-dimensionally[12-15]. This is because the Frank-Pryce structure and the RSS are almost spherically symmetric in contrast to the double twisted structure. In addition, it has been reported the double twisted structures, called 'toron' and

'hopfion' are formed when the Ch liquid crystals are confined to sandwich cells with strong homeotropic anchoring[16,17].

As we described above, owing to the strong anchoring conditions, the double twisted structures can be stabilized. In these cases, the structure is stabilized by controlling the director at the boundaries. On the other hand, typical textbooks on liquid crystals describe the anchoring force isn't necessary to realize the double twisted structure, which can be stabilized to decrease surface elasticity as well[5,9]. Here we show the double twisted structure constructed in the spherical Ch droplet with weak anchoring condition. The unique condition is realized in the isotropic-cholesteric (I-Ch) coexistence system. The detailed structure of the I-N or the I-Ch interface is mysterious; it has been suggested the pretransitional nematic ordering and the local biaxiality are induced at the interface[20-23]. On the other hand, the anchoring constant itself is estimated to be of the order of 10^{-6}-10^{-7} N/m as shown in references 24 and 25, which corresponds to the weak anchoring condition. Moreover, since the size of the droplets was several tens of micrometers, they can be directly observed with using conventional polarized microscopy. Changing the droplet size and the chirality, we investigated the stability of the double twisted structure in detail.

This paper is constructed as follows. Showing the experimental set-up in section II, we describe the physical properties of the double twisted structure in the spherical droplet obtained by the experiment in section III. Finally, in section IV, we give a theoretical explanation to the experimental results by the calculation of the Frank elastic free energy including the surface elastic term.

II. Experimental set-up

A. Sample preparation

We used the mixture of nematic compounds of 5CB (Merck) and No.270032 (LCC Ltd) with the weight ratio of 3:2 as the host sample, and added the chiral dopant of R811 (Merck). The concentration of R811 was 0.1~2.0wt.%, and the phase sequences of the mixture samples were Ch-54℃-I+Ch-58℃-I, not depending on the R811 concentration. Cooling the sample from the I phase, we made the Ch droplets in the coexistence phase. The size of the Ch droplets was controlled by the temperature within the I+Ch region, and we changed the droplet diameter from several to several tens of micrometers. On the other hand, the chirality strength was changed by the R811 concentration. The temperature of the sample was controlled by a commercial hot stage (Linkam).

To observe the texture of the Ch droplets, we prepared 50μm thickness cells sandwiched by two clean glass substrates. The glass plates were used just after washing without any further surface treatment. To measure the helical pitch length P_0 of the sample, we prepared the wedge-shaped cells using 150μm silica spacer and two glass plates coated with polyvinyl alcohol (Sigma-Aldrich) to realize the homogeneous anchoring. From the measurement, the relation between P_0 and the dopant concentration c was obtained as $P_0 = \beta/c$, where β is estimated to be 10.0 μm/wt.% in the isotropic-cholesteric coexistence state. The temperature and the concetration dependences of the helical pitch length P_0 are shown in Supplementary information 1. In addition, to measure the birefringence of the sample, we prepared a planar cell using 20μm PET film spacer and two glass plates coated with polyimide (AL1254, JSR).

B. Polarized optical microscopy

For the polarized optical microscopy (POM), we used the commercial microscopes of BX51

(Olympus) with the CCD camera (Thorlabs). Not only did we observe the texture of the sample, but we also measured the pitch wavenumber q in the double twisted structure embedded in the Ch droplets from the POM images. The simplest form to describe the director field in the structure can be

$$\mathbf{n} = (\sin qr \sin\phi, -\sin qr \cos\phi, \cos qr) \ , \quad (1)$$

where $r = \sqrt{x^2 + y^2}$ and $\phi = \arctan(y/x)$. Here, for simplicity, we assumed q doesn't depend on the coordinates r and z. When the incident light transmits along z axis through this director field, the transmitted light can be described analytically from the Jones matrix calculation[5]. Assuming the droplet is a complete sphere with radius R, we can describe the light transmission intensity profile under the crossed polarizer as

$$I(r,\phi) = I_0 \sin^2 2\phi \sin^2\left[\frac{2\pi}{\lambda}\sqrt{R^2 - r^2}\left(\frac{n_o n_e}{\sqrt{n_e^2 \cos^2 qr + n_o^2 \sin^2 qr}} - n_o\right)\right] , \quad (2)$$

where I_0 and λ are the intensity and the wavelength of the incident light, and n_e and n_o refractive index of extraordinary and ordinary light respectively. Averaging Eq.(2) over the ϕ direction, we obtain the 1-dimensional light transmission intensity profile along r direction:

$$I(r) = \frac{I_0}{2}\sin^2\left[\frac{2\pi}{\lambda}\sqrt{R^2 - r^2}\left(\frac{n_o n_e}{\sqrt{n_e^2 \cos^2 qr + n_o^2 \sin^2 qr}} - n_o\right)\right] . \quad (3)$$

Thus, fitting the profile $I(r)$ obtained from the POM image with Eq. (3), we can obtain q as a fitting parameter.

In this measurement, we used a band-path filter with the wavelength 530±10nm, so that we assumed the incident light was a monochromatic light with $\lambda \sim 530\text{nm}$. In addition, we measured the birefringence $\Delta n = n_e - n_o$ of the nematic mixture of 5CB and No.270032 in the

planar cell using a commercial spectroscope (USB2000+VIS-NIR, Ocean Optics). When a light transmits through a homogeneously aligned nematic liquid crystal under the crossed polarizer, the transmission intensity is described as[5]

$$I = I_0 \sin^2 2\Delta\phi \sin^2 \frac{\pi d \Delta n}{\lambda} , \quad (4)$$

where d is the cell thickness and $\Delta\phi$ the angle between the director and the polarizer. From this measurement, we obtained $\Delta n \sim 0.14$ for $\lambda = 530$nm in the I+Ch temperature region. In addition, $n_o \sim 1.5$ was given by reference[26].

To examine whether obtained POM images are explained by the assumed director field, we used the Jones matrix method[27]. In this method, the effect of the refraction and the diffractions are neglected. However, in this study, the characteristic textures on the droplets were mainly derived from the profiles of the polarization of the transmitted light, so that the POM images were well reproduced by the Jomes matrix method.

III. Experimental results

A. Phase diagram

In the previous work, we found two types of Ch droplets with stripe and concentric-circle (CC) texture appears in the coexistent state between the I and the Ch phase, which were called 'striped' and 'CC-type' droplets[28,29]. In addition to them, changing the droplet size and the chirality in the same system, we observed novel two types of droplets with rugby-ball and cross-like texture appear, and we called them 'rugby' and 'cross-type' droplets. The polarized optical microscope (POM) images of the four types of droplets are shown in Fig.2 (a)–(d).

First of all, we confirmed these droplets show almost spherical shape, while they are partially wetting to the cell substrate (Supplementary information 2 and 3). This indicates the interface

tension between the I and the Ch phase is enough strong to realize the spherical shape[24,30]. In the POM image the rugby-type droplet looks ellipsoidal and circular, which depends on the configuration of the polarizer and the analyzer as we show later (Fig.5 (a) and (b)). Thus, we measured the diameter of the rugby-type droplet only when it looks circular.

The stability of these four types of droplets depends on the droplet size and the chirality of the system. Figure 3 shows the phase diagram about the stability of the droplets with respect to the droplet diameter $2R$ and the chirality. We can find the rugby and the cross-type droplets appear when the droplet size and the chirality are low (group RC), and the striped and the CC-type droplets appear when they are high (group SC). The line in Fig.3 shows the helical pitch length P_0 of the sample, and it corresponds to the border line whether the group RC or SC becomes stable: the transition from the group RC to the SC occurs when $P_0 \sim 2R$.

In the group SC, the striped and the CC-type droplets randomly appear, so that we couldn't find out the condition whether the striped or the CC-type droplets become stable. From this result, it is indicated the free-energy difference in these droplets is extremely small. This is because the structural difference in the striped and the CC-type droplet is only the direction of the helical axis: the helical axis is parallel and perpendicular to the glass substrate in the striped and the CC-type droplet respectively[28]. In addition, we couldn't find out the condition whether the rugby or the cross-type droplets become stable in the group RC; thus, we assumed the structures of the rugby and the cross-type droplets are close to each other.

B. Structural analysis for rugby and cross-type droplets

In the striped droplet, since the period of the stripe texture agrees with helical half pitch length, the texture indicates the periodic helical structure of the Ch phase[28]. As shown in Fig.4

(a)–(e) and supplementary information4(a) and (b) (S4(a) and S4(b).wmv), in the cooling process within the I+Ch phase, the rugby-type droplet grows, and when $2R$ becomes larger than P_0, it transits to the striped or the CC-type droplet. Since the transition to the striped droplet occurs continuously, we can consider the helical axis is extending parallel to the glass substrate in the rugby-type droplet.

To reveal the director field in the rugby-type droplet, we observed the droplet by polarized microscope, changing polarizer P and analyzer A as shown in Fig.5(a). The droplet looks brightest when $(P, A) = (30^\circ, 120^\circ), (120^\circ, 30^\circ)$, and darkest when $(P, A) = (30^\circ, 30^\circ), (120^\circ, 120^\circ)$, that is, brightest and darkest with crossed and parallel polarizer respectively. This indicates the director was almost twisted 90 degrees along z axis and the polarization of the light rotated 90 degrees through the droplet owing to the wave-guide effect[31]. Thus, the helical axis is extending perpendicular to the glass substrate in the rugby-type droplet. On the other hand, since the rugby-ball-like texture indicates the periodic helical structure, the axis is also extending parallel to the substrate simultaneously. Therefore, the helical axis should be extending in the two directions, which indicates the double twisted helical structure is embedded in the rugby-type droplet as shown in Fig.6(a). Thus, assuming the double twisted structure described in Fig.6(a) as the director field, we numerically calculated the light transmitted intensity profiles in the rugby-type droplet using Jones matrix method[27] as shown in Fig.5(b). Since the obtained images are consistent with Fig.5(a), we can confirm the double twisted structure is surely embedded in the droplet. Moreover, in the system with the strong anchoring condition, similar texture has been reported when the double twisted structure is formed[12,13]. The structure described in Fig.6(a) well explains the continuous transition from the rugby to the striped and the CC-type droplet where the helical axis is parallel and perpendicular to the glass substrate respectively

(Fig.4 (a)–(e)): the axis is extending in both parallel and perpendicular direction to the substrate in the rugby-type droplet, and one of them is selected when the transition occurs.

On the other hand, the cross-type droplet continuously transits to the striped droplet as shown in Fig.4(f)–(j) and supplementary information4(c) (S4(c).wmv), while not to the CC-type droplet. This result indicates the helical axis is not extending perpendicular to the substrate in the cross-type droplet. In addition, since the structure of the cross-type droplet is similar to the rugby-type droplet as we described in section III-A, the double-twisted structure should be also embedded in the cross-type droplet, and it is considered the helical axes are radially extending in the plane parallel to the substrate as shown in Fig.6(b). As shown in Fig.7(a), in the polarized microscopy, the direction of the cross-like texture rotates when the polarizer and the analyzer rotate with crossed polarizer. This indicates the director field is radially symmetric in the plane parallel to the substrate as shown by Fig.6(b). Calculating the light transmitting intensity profiles under the director configuration in Fig.6(b), we found the cross-like textures are well-reproduced as shown in Fig.7(b). Therefore, we concluded the double twisted structure is also embedded in the cross-type droplet as well as the rugby-type droplet.

In summary, the double twisted structure is embedded in the rugby and the cross-type droplets, while the single helix structure in the striped and the CC-type droplets. The transition from the double twisted to the single helix structure occurs when the helical pitch length P_0 goes beyond the droplet diameter $2R$ as shown in Fig.3. Here, it should be noted P_0 is the pitch length under the assumption that the single helix structure is formed. If the double twisted structure is formed with the same material, the pitch length P disagrees with P_0. We discuss this point in detail, in the following section.

C. Pitch wavenumber in double twisted structure

In the double twisted structure, the equilibrium pitch length $P = 2\pi/q$ disagrees with the pitch length in the bulk Ch liquid crystal with the single helix structure $P_0 = 2\pi/q_0$ [5]. To measure q, we made the 1-dimensional light transmission intensity profile $I(r)$ from the POM image of the cross-type droplet as shown in Fig.8(a) and (b). In this droplet, since the helical axes are radially extending in the plane perpendicular to the incident light, $I(r)$ should be described by Eq.(3). As shown in Fig.8(b), $I(r)$ fitted well with Eq.(3), so that we successfully obtained q as a fitting parameter. Here, it should be noted q can depend on the coordinates r and z, while we neglected this dependency when we assumed the director field in Eq.(1). Neglecting r and z dependence of q, we can well explain the experimental result as shown in Fig. 8(b); this verify the Eq.(1) can be a good approximation for this study.

Here, for convenience, we define the non-dimensional parameter α as

$$\alpha = \frac{q}{q_0} . \quad (5)$$

From the measurement, we found α decreases as $2q_0R$ increases as shown in Fig.9. The measured α were well fitted with a common curve, not depending on the concentration of R811; this means the pitch wavenumber q is determined only by $2q_0R$.

IV. Theoretical analysis

In the droplets of our system, defects weren't observed. Thus, assuming the scholar order parameter is constant in the droplet, we only calculate the elastic energy derived from the director deformation in this paper. The Frank elastic free energy density in the Ch phase is described as[9]

$$f = \frac{1}{2}K_1(\mathrm{div}\mathbf{n})^2 + \frac{1}{2}K_2(\mathbf{n}\cdot\mathrm{rot}\mathbf{n} + q_0)^2 + \frac{1}{2}K_3 \mid \mathbf{n}\times\mathrm{rot}\mathbf{n} \mid^2 - \frac{1}{2}(K_2 + K_{24})\mathrm{div}(\mathbf{n}(\mathrm{div}\mathbf{n}) + \mathbf{n}\times\mathrm{rot}\mathbf{n}) \quad , \quad (6)$$

where K_1, K_2, K_3 and K_{24} are the splay, the twist, the bend and the saddle-splay elastic constant respectively. The saddle-splay term in Eq.(6) is negligible when we consider the deformation in the bulk Ch liquid crystals, since it is convertible to a surface integral over the interface. However, in our system, this term cannot be negligible because the droplet diameter $2R$ is comparable with the helical pitch length $2\pi/q$ which is a characteristic length of the director deformation. Moreover, owing to the saddle-splay term, the double twisted structure is stabilized[9].

Assuming the double twisted structure described by Eq.(1) as the director field, we calculated the elastic free energy density described by Eq.(6),

$$f = \frac{K_2}{2}\left[\left(q^2 + \frac{\sin^2 2qr}{4r^2}\right) - q_0\left(2q + \frac{\sin 2qr}{r}\right) + q_0^2\right] + \frac{K_3}{2}\frac{\sin^4 qr}{r^2} - \frac{K_{24}}{2}\frac{q\sin 2qr}{r} \quad . \quad (7)$$

For simplicity, we expanded Eq. (7) to second order in qr,

$$f \sim \left(\frac{K_2}{2} - 2K_2\alpha + (K_2 - K_{24})\alpha^2\right)q_0^2 + \left[\frac{2K_2}{3}\alpha^3 + \left(-\frac{2(K_2 - K_{24})}{3} + \frac{K_3}{2}\right)\alpha^4\right]q_0^4 r^2 \quad , \quad (8)$$

where we used Eq. (5) for convenience. Integrating Eq. (8) over the spherical region with radius R, we get the total free energy,

$$F \sim \frac{4\pi q_0^2 R^3}{3}\left[\frac{K_2}{2}(1-2\alpha)^2 - (K_2 + K_{24})\alpha^2 + \frac{4K_2(\alpha^3 - 2\alpha^4)}{15}q_0^2R^2 + \frac{(4(K_2 + K_{24}) + 3K_3)\alpha^4}{15}q_0^2R^2\right] . \quad (9)$$

For strict analysis, it should be better to calculate the anchoring energy at the interface between the I and the Ch phase in addition to Eq.(9). However, in our system, the extrapolation length

can be estimated to be of the order of 10^0-10^2 μm from references 5,9,24 and 25, which includes the range where the length is at least one order larger than P and R. In this paper, adopting the simplest assumption, we neglect the anchoring force. As we show later in this section, the experimental results are well explained under this assumption.

In Eq.(9), the first and the second term are derived from the twist and the saddle-splay deformation. When $2q_0R << 1$, α and the free energy are determined by these terms,

$$\alpha = \frac{K_2}{K_2 - K_{24}} \quad , \quad (10a)$$

$$F = -\frac{4\pi q_0^2 R^3}{3}\left(\frac{K_2(K_2 + K_{24})}{2(K_2 - K_{24})}\right) < 0 \quad . \quad (10b)$$

Since the elastic energy in the single helix structure is zero in Eq. (6), Eq. (10b) means the double twisted structure is more stable than the single helix. The double twisted structure is stabilized to decrease the elastic energy derived from the saddle-splay deformation; this is the prevalent theory which explains why the structure is realized[5,6,9, 32, 33].

On the other hand, as $2q_0R$ increases, the free energy increases owing to the last term in Eq. (9), which means the elastic energy derived from the saddle-splay and the bend deformation increases. Thus, the double-twisted structure is gradually destabilized as $2q_0R$ increases, and it transits to the single helix structure at a certain $2q_0R$ value. The stability of the double twisted structure is mainly determined by the competition between the saddle-splay and the bend deformation.

α is determined by minimizing the free energy described by Eq.(9) ($\partial F/\partial\alpha = 0$). Using the non-dimensional parameters as defined below,

$$k_2 = \frac{3K_2}{-4(K_2 - K_{24}) + 3K_3} \quad , \quad (11a)$$

$$k_{24} = \frac{3K_{24}}{-4(K_2 - K_{24}) + 3K_3} \quad , \quad (11b)$$

we obtain

$$\alpha(q_0R, k_2, k_{24}) = -\frac{k_2}{3} + \frac{1}{q_0R}\left[\left(\frac{B}{2} + \sqrt{\frac{B^2}{4} + \frac{A^3}{27}}\right)^{\frac{1}{3}} + \left(\frac{B}{2} - \sqrt{\frac{B^2}{4} + \frac{A^3}{27}}\right)^{\frac{1}{3}}\right] \quad , \quad (12)$$

$$A(q_0R, k_2, k_{24}) = \frac{5(k_2 - k_{24})}{2} - \frac{k_2^2}{3}q_0^2R^2 \quad , \quad (13a)$$

$$B(q_0R, k_2, k_{24}) = \frac{5k_2}{2} + \frac{5k_2(k_2 - k_{24})}{6}q_0R - \frac{2k_2^3}{27}q_0^3R^3 \quad . \quad (13b)$$

As shown in Fig.9, since the α values obtained from the experiments were well fit with Eqs.(12),(13a) and (13b), the validity of our analysis is experimentally verified. From the fitting parameters k_2 and k_{24}, we obtained $K_{24}/K_2 \sim 0.85$ and $K_3/K_2 \sim 1.9$, which are consistent with the values reported in references[34-36].

Finally, using Eqs.(9), (11)–(13) and the K_{24}/K_2 and the K_3/K_2 values obtained above, we calculated the $2q_0R$ dependence of the free energy. As shown in Fig. 10, the free energy becomes zero when $2q_0R \sim 6.6 \sim 2\pi$. This means the transition from the double twisted to the single helix structure occurs when $2R \sim P_0$, which consists with the phase diagram in Fig. 3.

V. Conclusion

In this paper, we found the double twisted structure is formed in the spherical Ch droplets, and examined its stability with changing the droplet diameter $2R$ and the chirality. When the droplet size is small, the double twisted structure is stable. However, as the size increases, it is gradually destabilized, and transits into the single helix structure when the helical pitch length $2\pi/q_0$ goes

beyond the droplet diameter ($2q_0R \sim 2\pi$). Simultaneously, we theoretically analyzed the stability of the double twisted structure by calculating the Frank elastic free energy including the saddle-splay term as given by Eq. (9). As a result, the stability is determined by the competition between the saddle-splay and the bend deformation, in other words, the surface and the bulk elastic term. This analysis well explained the experimental results described above.

Here, it should be noted the anchoring energy at the I-Ch interface is neglected: the anchoring force is not required to realize the double twisted structure. Just being confined to a small region, the structure is stabilized; this is because the contribution from the surface elasticity becomes larger than the bulk elasticity in this situation. On the other hand, as the droplet size increases, since the contribution from the bulk elasticity increases, the double twisted structure is gradually destabilized. When the region attains a certain size where the surface elastic energy balances the bulk energy, the system transits from the double twisted to the single helix structure to minimize the total free energy.

Acknowledgement

We are grateful to Dr. Isa Nishiyama of DIC corporation for variable comments and discussions. This work was supported by JSPS NEXT program and JSPS KAKENHI Grant Number 15K17739.

References

1 H. Kikuchi, M. Yokota, Y. Hisakado, H. Yang and T. Kajiyama, *Nat. Mater.*, 2002, **1**, 64

2 S. Yokoyama, S. Mashiko, H. Kikuchi, K. Uchida, and T. Nagamura, *Adv. Mater.*, 2006, **18**,

48

3 Z. Ge, S. Gauza, M. Ziao, H. Xianyu, and S. -T. Wu. *Appl. Phys. Lett*., 2009, **94**, 101104

4 W. Cao, A.Muñoz, P. Palffy-Muhoray, and B. Taheri, *Nat.Mater*., 2002, **1**, 111

5 M. Kleman and O. D. Lavrentovich, *Soft Matter Physics An Introduction*, Springer, 2003

6 D. C. Wright and N. D. Mermin, Rev. Mod. Phys., 1989, **61**, 385

7 O. Henrich, K. Stratford, M. E. Cates, and D. Marenduzzo, *Phys. Rev. Lett.*, 2011, **106**, 107801

8 J. Fukuda and S. Žumer, Nat. Commun., 2011, **2**, 246

9 P. G. de Gennes and J. Prost, *The Phisics of Liquid Crystals second edition*, Clarendon Press Oxford, 1993

10 M. Ambrožič and S. Žumer, *Phys. Rev. E*, 1999, **59**, 4153

11 E. Enz and J. Lagerwall, *J. Matter. Chem*., 2010, **20**, 6866

12 F. Xu and P. P. Crooker, *Phys. Rev. E*, 1997, **56**, 6853

13 D. Seč, T. Porenta, M. Ravnik, and S. Žumer, *Soft Matter*, 2012, **8**, 11982

14 Y. Bouligand, F. Livolant, *J. Phys. (Paris)*, 1984, **45**, 1899

15 S. Candau, P. Le Roy, and F. Debeauvais, *Mol. Cryst. Liq. Cryst.*, 1973, **23**, 283

16 I. I. Smalyukh, Ivan, Y. Lansac, N. A. Clark and R. P. Trivedi, *Nat. Mater.*, 2010, **9**, 139

17 T. Porenta, S. Čopar, P. J. Ackerman, M. B. Pandey, M. C. M. Varney, I. I. Smalyukh and S. Žumer, *Sci. Rep.*, 2014, **4**, 7337

18 O. J. Dammone, I. Zacharoudiou, R. P. A. Dullens, J. M. Yeomans, M. P. Lettinga, and D. G. A. L. Aarts, *Phys. Rev. Lett.*, 2012, **109**, 108303

19 A. H. Lewis, I. Garlea, J. Alvarado, O. J. Dammone, P. D. Howell, A. Majumdar, B. M.

Mulder, M. P. Lettinga, G. H. Koenderinkb and D. G. A. L. Aarts, *Soft Matter*, 2014, **10**, 7865

20 S. Immerschitt, T. Koch, W. Stille, and G. Strobl, *J. Chem. Phys.*, 1992, **96**, 6249

21 Z. Y. Chen, *Phys. Rev. E*, 1993, **47**, 3765

22 R. V. Roij, M. Dijkstra and R. Evans, *Europhys. Lett*, 2000, **49**, 350

23 M. P. Allen, J. Chem. Phys., 2000, **112**, 5447

24 S. Faetti and V. Palleschi *Phys. Rev .A*, 1984, **30**, 3241

25 H. Yokoyama, S. Kobayashi and H. Kamei, *Mol. Cryst. Liq. Cryst.*, 1984, **107**, 31126 J. Li, S. Gauzia and S -T. Wu, *Opt. Express*, 2004, **12**, 2002,

27 R. C. Jones, *J. Opt. Soc. Am.*, 1941, **31**, 488

28 J. Yoshioka, F. Ito, Y. Suzuki, H. Takahashi, H. Takizawa and Y. Tabe, *Soft Matter*, 2014, **10**, 5869

29 P. Oswald and S. Dequidt, *Phys. Rev. Lett.*, 2008, **100**, 217802

30 H. Yokoyama, S. Kobayashi and H. Kamei, *Mol. Cryst. Liq. Cryst.*, 1985, **129**, 109

31 C. H. Gooch, and H. A. Tarry, *J. Phys. D: Appl. Phys.* 1975, **8**, 1575

32 S. Meiboom, J. P. Sethna, P. W. Anderson and W. F. Brinkman, *Phys. Rev. Lett.* 1981, **46**, 1216

33 J. Fukuda, *Phys. Rev. E*, 2012, **85**, 020701

34 D. W. Allender, G.P. Crawfors ad J. W. Doane, *Phys. Rev. Lett.*, 1991, **67**, 1442

35 R. D. Polak, G. P. Crawford, B. C. Kostival, J. W. Doane and S. Žumer, *Phys. Rev. E*, 1994, **49**, R978

36 D. R. Link, M. Nakata, Y. Takanishi, K. Ishikawa and H. Takezoe, *Phys. Rev. Lett.*, 2001, **87**, 195507

Figure caption

Figure 1. Schematic image of the director configuration in (a) single helix and (b) double twisted structures. In the double twisted structure, the helical axes are extending radially within a plane.

Figure 2. Polarized optical microscope (POM) image of four types of Ch droplets. (a) Rugby-type droplet. (b) Cross-type droplet. (c) Striped droplet. (d) CC-type droplet.

Figure 3. Phase diagram about the stability of Ch droplets with respect to droplet diameter $2R$ and concentration of R811 c. The solid line shows the helical pitch length in bulk $P_0 = \beta / c$, where $\beta = 10.0\mu\text{m} / \text{wt.\%}$.

Figure 4. (a)–(e) POM images of the transition from rugby-type to CC-type and striped droplet. (f)–(j) POM images of the transition from cross-type to striped droplet.

Figure 5. (a) POM images of rugby-type droplet. The arrows in the figure indicate the direction of polarizer and analyzer. The concentration of R811 was 0.3wt.%. (b) Transmitted light intensity profile calculated by Jones matrix method under the assumption of double twisted structure. The assumed director field is $n_x = -\sin q_0 r \sin\theta \cos\phi_0 + \cos q_0 r \sin\phi_0$, $n_y = \sin q_0 r \sin\theta \sin\phi_0 + \cos q_0 r \cos\phi_0$, $n_z = \sin q_0 r \cos\theta$, where $r = \sqrt{x^2 + z^2}$ and $\theta = \arctan(x/z)$ in the coordinate system shown in left-top corner. ϕ_0 is the angle between x and the helical axis in the xy-plane.

Figure 6. Director configuration in (a) rugby and (b) cross-type droplet. The right-down figures in (a) and (b) show the schematic image of the two-types of the droplets, where $\mathbf{h_1}$ and the $\mathbf{h_2}$ show the two directions of helical axis in the double twisted structure. The left-down and right-up figures in (a) and (b) show the side and top view of the director configuration in the rugby and the cross-type droplet respectively.

Figure 7. (a) POM images of cross-type droplet. The arrows in the figure indicate the direction of polarizer and analyzer. The concentration of R811 was 0.3wt.%. (b) Transmitted light intensity profile calculated by Jones matrix method under the assumption of double twisted structure. The assumed director field is $n_x = \sin q_0 r \sin\theta$, $n_y = -\sin q_0 r \cos\theta$, $n_z = \cos q_0 r$, where $r = \sqrt{x^2 + y^2}$ and $\theta = \arctan(y/x)$ in the coordinate system shown in left-top corner.

Figure 8. (a)2D and (b)1D light transmission intensity profiles in cross-type droplet. From the circular average of the POM image (a), we obtained $I(r)$ (b). The solid line in (b) is fitted using Eq. (3).

Figure 9. $2q_0R$ dependence of α with various R811 concentration. Here, α is defined as q/q_0 , where q is the pitch wavenumber of the double twisted structure, and q_0 the wavenumber under the assumption of the single helix. The solid line is fitted using Eqs.(12), (13a) and (13b). The fitting parameters are $k_2 \sim 0.58$ and $k_2 - k_{24} \sim 0.088$, from which we

obtain $K_{24}/K_2 \sim 0.85$ and $K_3/K_2 \sim 1.9$.

Figure 10. $2q_0R$ dependence of elastic free energy in double twisted and single helix structure. The solid line shows the normalized free energy $3F/(4\pi K_2 q_0^2 R^3)$ calculated from Eqs. (9),(11)–(13), $K_{24}/K_2 = 0.85$ and $K_3/K_2 = 1.9$. The broken line shows the energy in the single helix structure, that is, zero. $3F/(4\pi K_2 q_0^2 R^3)$ goes beyond zero when $2q_0R \sim 6.6$.

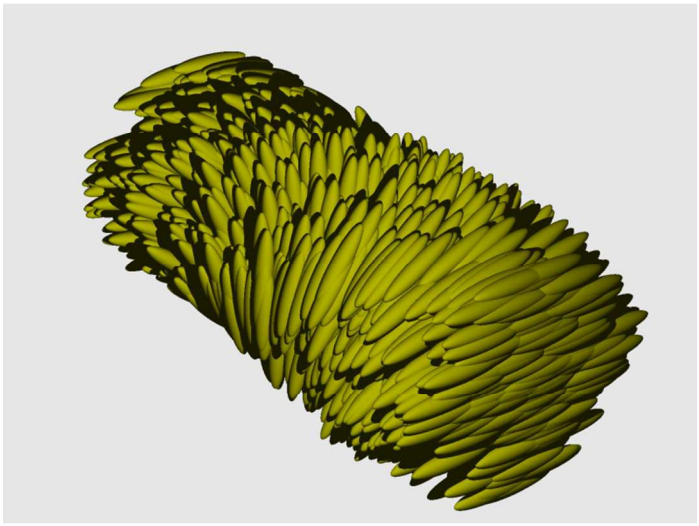

(a)

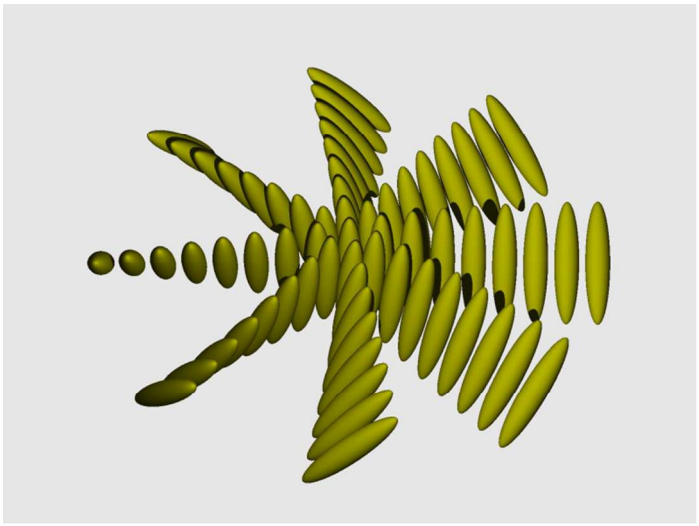

(b)

Fig.1

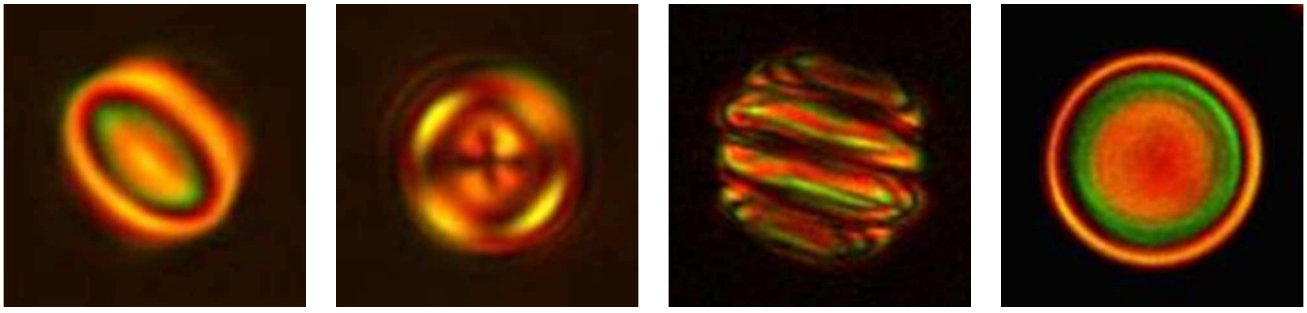

(a) (b) (c) (d)

Fig.2

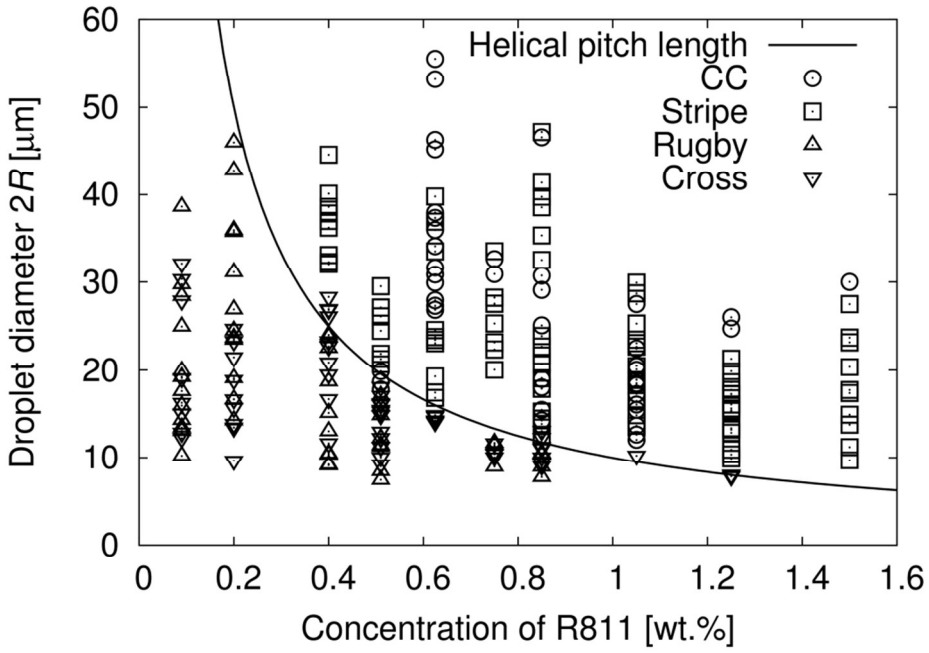

Fig.3

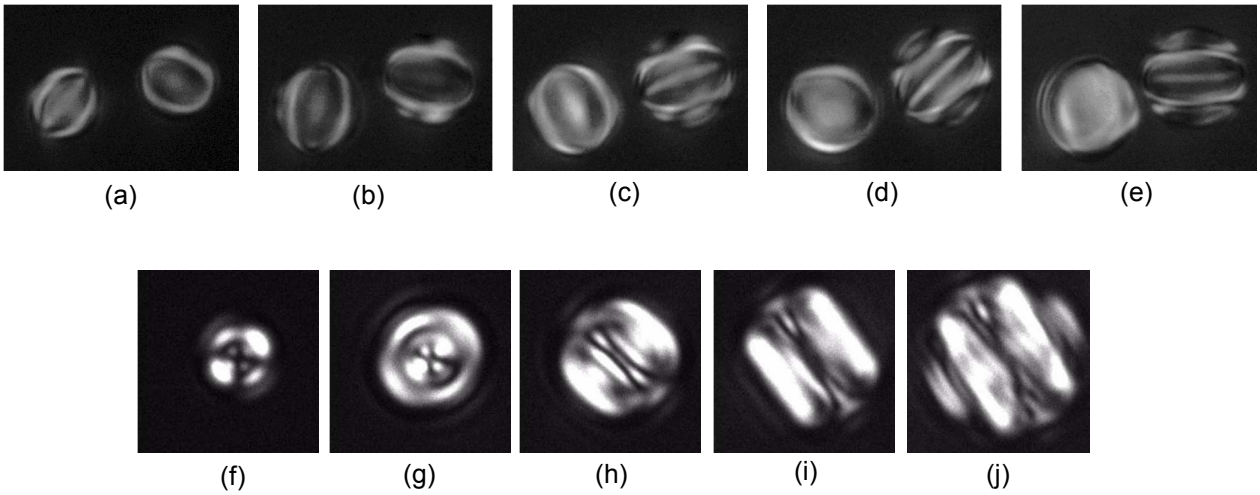

Fig.4

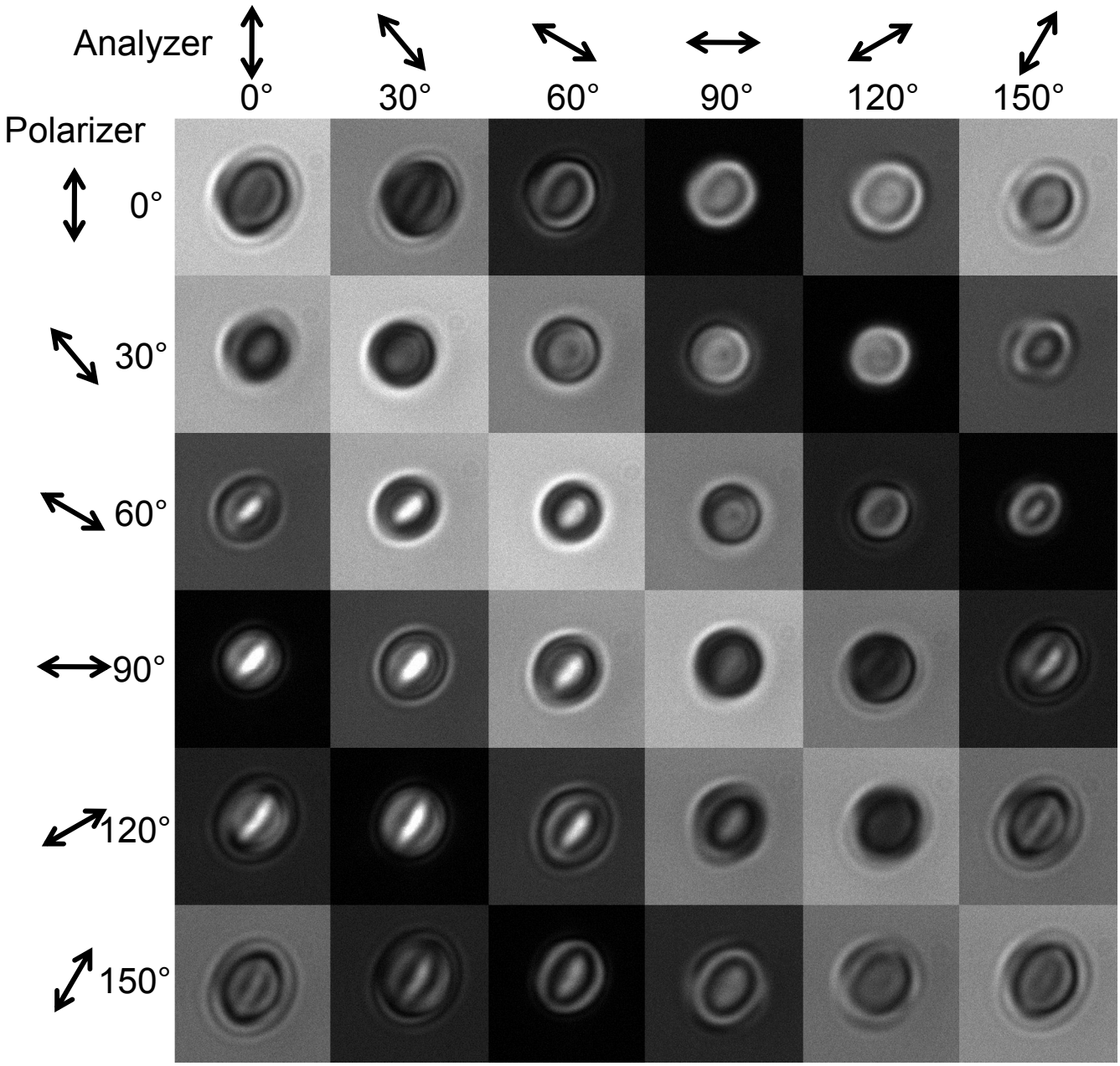

(a)

Fig.5

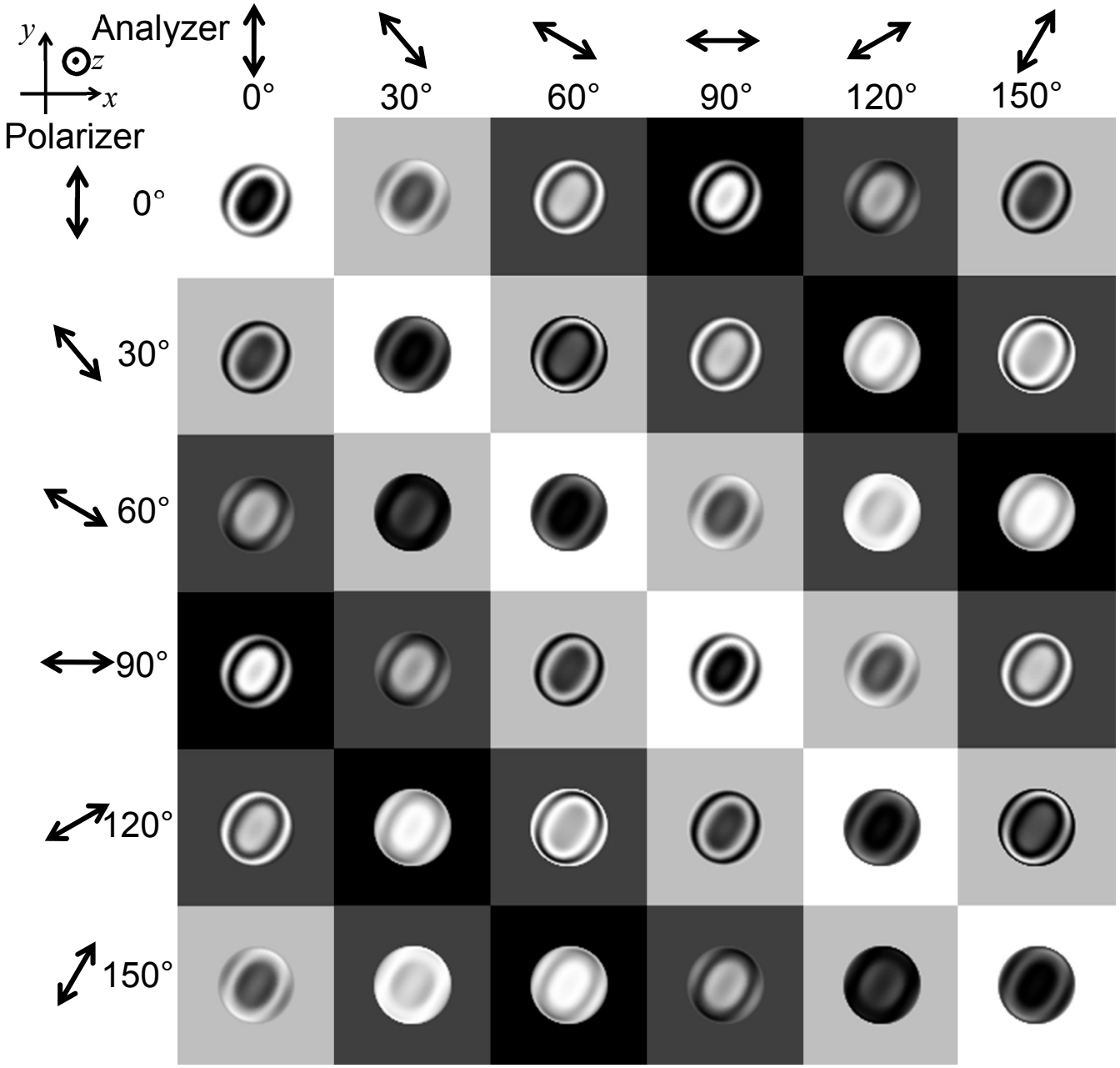

(b)

Fig.5

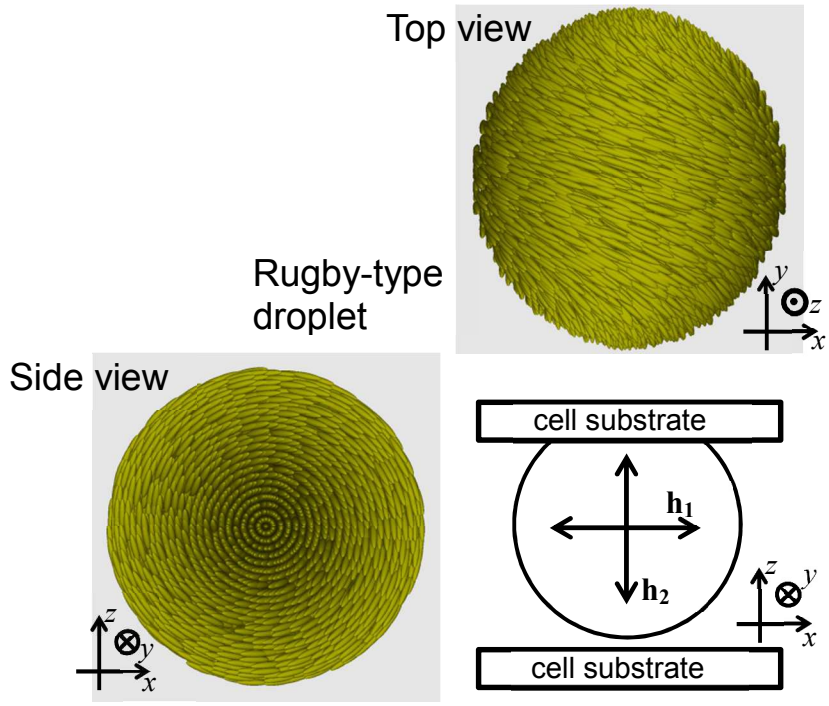

(a)

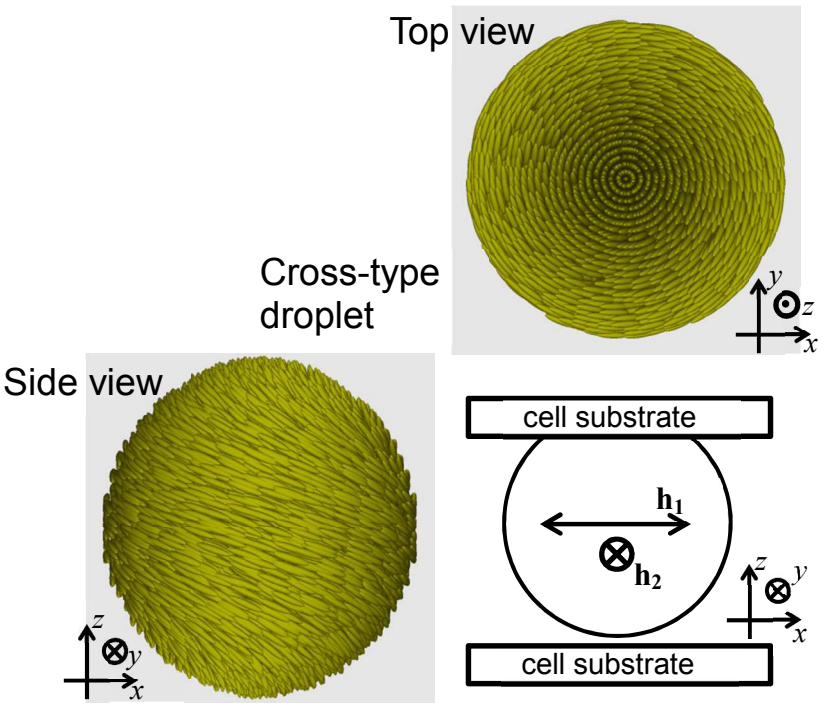

(b)

Fig.6

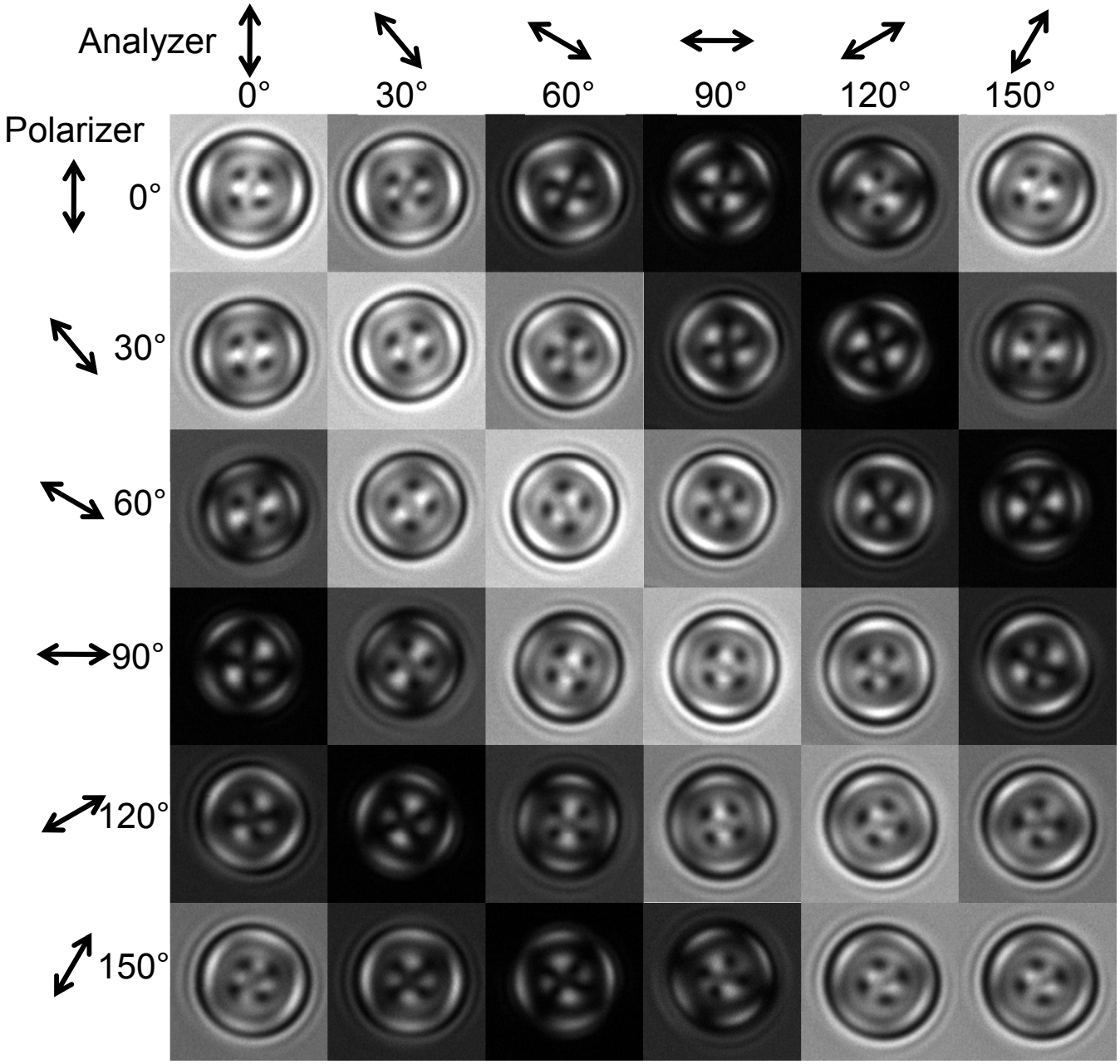

Fig.7

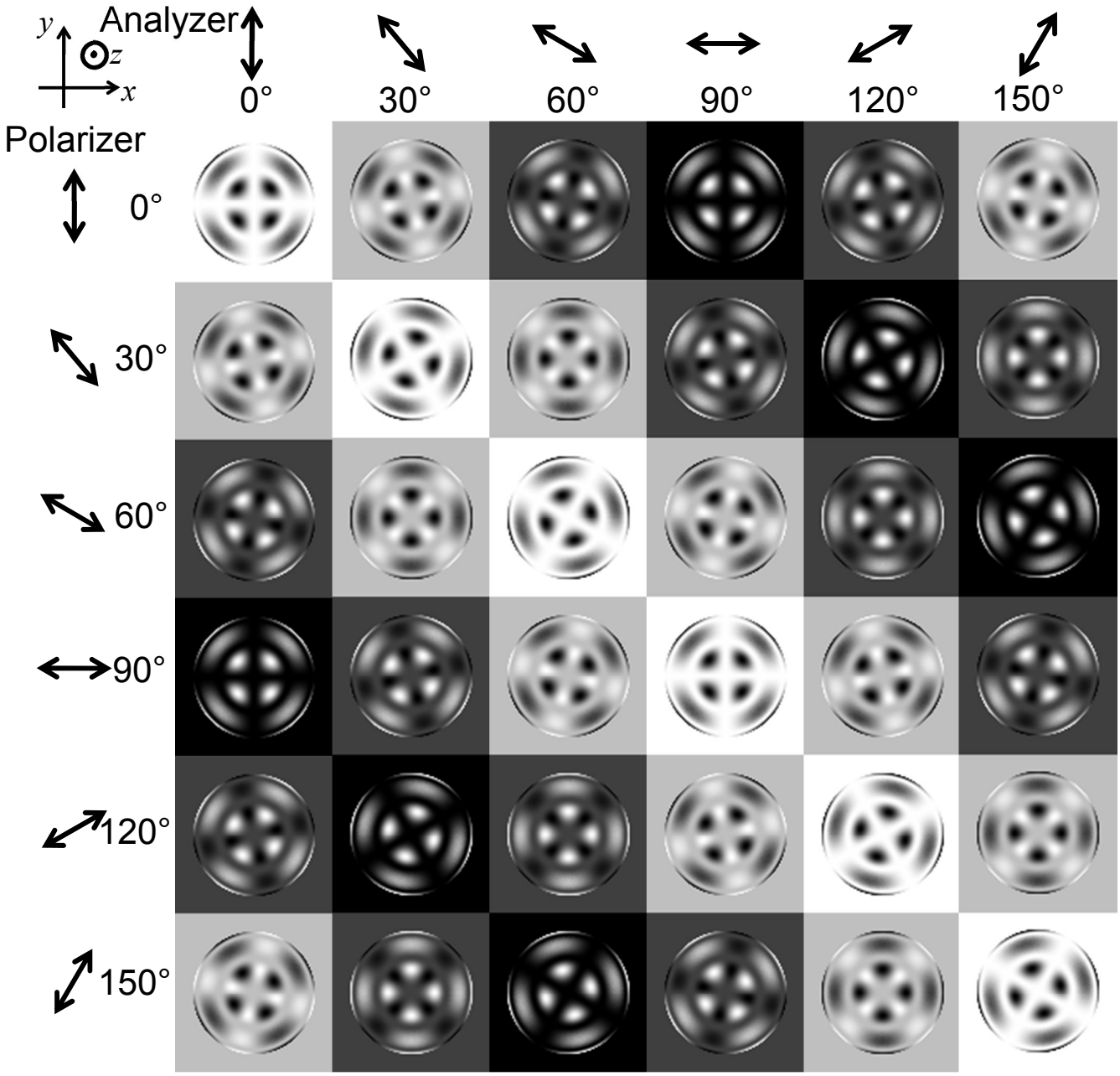

(b)

Fig.7

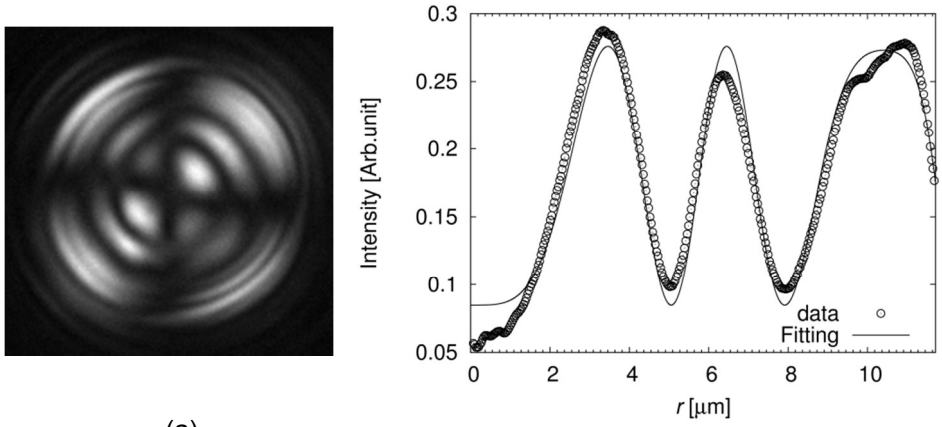

(a) (b)

Fig.8

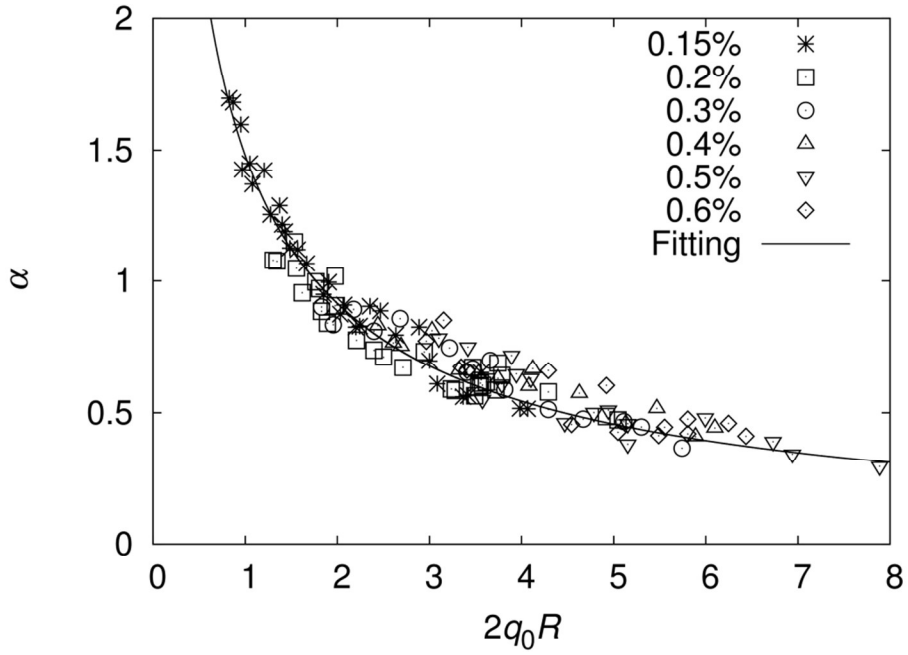

Fig.9

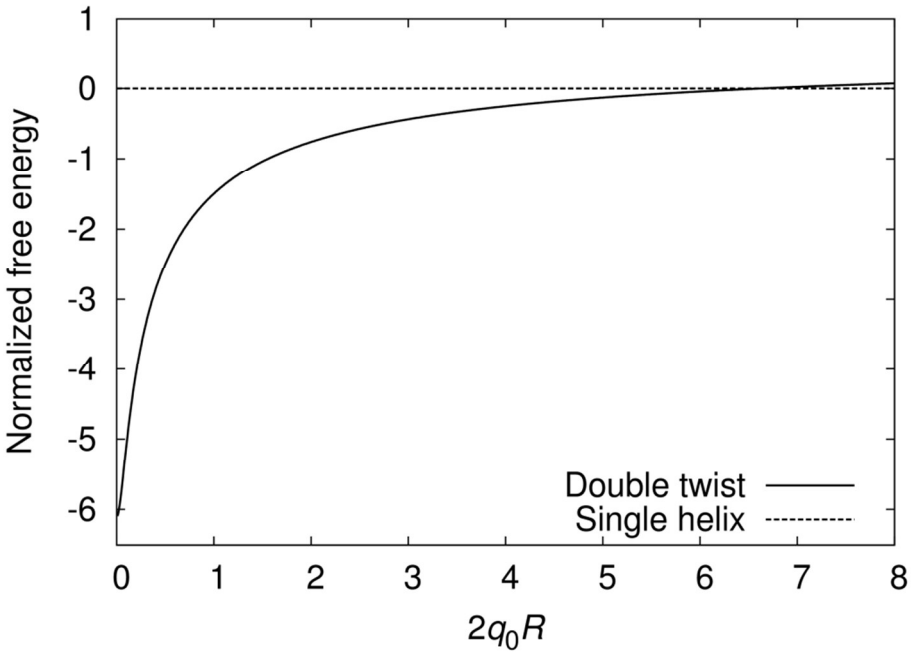

Fig.10

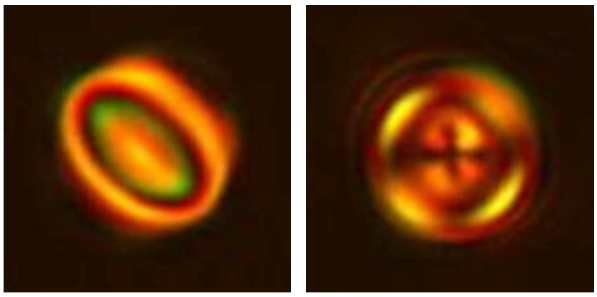

The stability of the double twisted structure formed in spherical cholesteric droplets under weak anchoring condition was analyzed.